Anomalous Diffusion of Major Histocompatibility Complex Class I Molecules on HeLa Cells Determined by Single Particle Tracking

Patricia R. Smith, Ian E. G. Morrison, Keith M. Wilson, Nelson Fernández, and Richard J. Cherry
Department of Biological Sciences, University of Essex, Colchester CO4 3SQ, England

ABSTRACT Single-particle tracking (SPT) was used to determine the mobility characteristics of MHC (major histocompatibility complex) class I molecules at the surface of HeLa cells at 22°C and on different time scales. MHC class I was labeled using the Fab fragment of a monoclonal antibody (W6/32), covalently bound to either R-phycoerythrin or fluorescent microspheres, and the particles were tracked using high-sensitivity fluorescence imaging. Analysis of the data for a fixed time interval suggests a reasonable fit to a random diffusion model. The best fit values of the diffusion coefficient D decreased markedly, however, with increasing time interval, demonstrating the existence of anomalous diffusion. Further analysis of the data shows that the diffusion is anomalous over the complete time range investigated, 4–300 s. Fitting the results obtained with the R-phycoerythrin probe to $D = D_0 t^{\alpha-1}$, where D_o is a constant and t is the time, gave $D_0 = (6.7 \pm 4.5) \times 10^{-11}$ cm^2 s^{-1} and $\alpha = 0.49 \pm 0.16$. Experiments with fluorescent microspheres were less reproducible and gave slower anomalous diffusion. The R-phycoerythrin probe is considered more reliable for fluorescent SPT because it is small (11 × 8 nm) and monovalent. The type of motion exhibited by the class I molecules will greatly affect their ability to migrate in the plane of the membrane. Anomalous diffusion, in particular, greatly reduces the distance a class I molecule can travel on the time scale of minutes. The present data are discussed in relation to the possible role of diffusion and clustering in T-cell activation.

INTRODUCTION

The major histocompatibility complex (MHC) class I molecules, which present antigenic peptides to T cells, are noncovalently associated trimolecular complexes consisting of the class I MHC heavy chain, β_2-microglobulin (β_2m), and antigenic peptide (Bjorkman et al., 1987). Class I molecules bind peptides derived from viruses or bacteria living in the cytosol and present them at the cell surface to CD8$^+$ T cells. These transmembrane glycoproteins are expressed on almost all nucleated cells, with varying levels of expression from $\sim 10^3$ to 10^6 per cell (Fernández et al., 1992). Membrane proteins are often able to diffuse within the plane of a cell membrane, and so can potentially form dynamic associations. The dimerization of membrane receptors in response to a particular stimulus is an important mechanism in, for example, transmembrane signaling (Bormann and Engelman, 1992; Metzger, 1992; Heldin, 1995) and the activation of immunological receptors (Weiss and Littman, 1994). Clustering of MHC molecules has been observed with MHC class I and could be involved in T-cell activation (Matkó et al., 1994; Capps et al., 1993; Chakrabarti et al., 1992; Weng and DeLisi, 1998).

The lateral mobility of a wide variety of membrane proteins has been investigated by the method of fluorescence recovery after photobleaching (FRAP) (Jovin and Vaz, 1989; Peters and Scholz, 1991; Zhang et al., 1993). In common with many cell surface receptors, FRAP measurements of MHC class I and MHC class II molecules have indicated the presence of both a mobile population and a fraction that is immobile over the time scale of the experiment (Damjanovich et al., 1983; Edidin and Stroynowski, 1991; Wade et al., 1989; Qiu et al., 1996). More recently, the technique of single particle tracking (SPT) has been employed to gain further insight into how proteins move on cell surfaces (for reviews, see Cherry, 1992; Sheets et al., 1995; Saxton and Jacobson, 1997). SPT involves attaching a small particle, typically 12–40 nm in diameter, to the cell surface receptor of interest. Two types of particle have been utilized: fluorescent particles, which are imaged by low-light-level fluorescence microscopy (Gross and Webb, 1988; Anderson et al., 1992; Wang et al., 1994; Ghosh and Webb, 1994; Hicks and Angelides, 1995; Wilson et al., 1996), and gold particles, which are imaged by differential interference contrast microscopy (Sheetz et al., 1989; de Brabander et al., 1991; Lee et al., 1991; Kusumi et al., 1993; Sako and Kusumi, 1994; Simson et al., 1995). The movement of individual proteins in the plasma membrane of living cells can be monitored by tracking the particle positions through a sequence of images. Provided that particles are well separated compared with the resolution of the optical microscope, the positions of the particles can be determined with high precision, so that the spatial resolution of the technique is on the order of 10–20 nm (compared with ~ 1 μm in a FRAP experiment). SPT of single fluorescent molecules has been achieved for lipids in a model system (Schmidt et al., 1996; Schütz et al., 1997a).

SPT measurements have now been performed with a number of receptors on different cell types. In all cases investigated so far, departures from simple diffusion have been detected. In addition to random motion, both directed motion and constrained diffusion have been observed, and

Received for publication 13 October 1998 and in final form 10 March 1999.

Address reprint requests to Dr. Richard J. Cherry, Department of Biological Sciences, University of Essex, Colchester CO4 3SQ, England. Tel.: +44-0-1206-872244; Fax: +44--0-1206-872592: E-mail: cherr@essex.ac.uk.

0006-3495/99/06/3331/14 $2.00

in some cases all three types of motion are apparently present on the same cell (Kusumi et al., 1993; Wilson et al., 1996; Simson et al., 1998). In the case of constrained diffusion, two different interpretations of the phenomenon have emerged. In one model, receptors move randomly within submicrometer domains, their long-range diffusion determined by the rate at which they can escape from these domains (Sako and Kusumi, 1994, 1995; Kusumi and Sako, 1996). In a related model, receptors undergo random diffusion interspersed with periods of temporary confinement (Simson et al., 1995, 1998). Some FRAP experiments have also been interpreted by a domain model (Edidin and Stroynowski, 1991; Schram et al., 1994). Alternatively, constrained diffusion may be interpreted by an anomalous diffusion model. Anomalous diffusion in cell membranes may result from obstacles and traps with a broad distribution of binding energies or escape times (Saxton, 1996). SPT measurements with fluorescent low-density lipoprotein (LDL) particles have provided evidence for this type of motion (Ghosh and Webb, 1990; Ghosh, 1991; Slattery, 1995). Feder et al. (1996) have recently applied an anomalous diffusion model to the interpretation of FRAP experiments. They show that FRAP data may be fitted equally well by this model as by the conventional method of separating the recovery curve into mobile and immobile fractions.

We have previously reported fluorescence SPT measurements with MHC class I on HeLa cells (Cherry et al., 1997) and MHC class II on transfected fibroblasts (Wilson et al., 1996). Somewhat unexpectedly, we observed very low mobilities for these molecules. Although evidence was obtained for different modes of motion, molecules apparently undergoing random diffusion had diffusion coefficients on the order of 10^{-12} cm^2 s^{-1}. In the present study, we have carried out experiments on MHC class I on HeLa cells to determine whether this low mobility can be reconciled with the higher mobilities more commonly observed with FRAP and SPT experiments. We also compare the utility of a phycobiliprotein, R-phycoerythrin (PhyE), with fluorescent latex microspheres for SPT experiments. We have performed these measurements with MHC class I on HeLa cells because directed motion is rarely observed with this system, which considerably simplifies the data analysis. We show that diffusion is anomalous over a wide time range and that the previously reported low diffusion coefficients are a consequence of the long time scale of those measurements. These findings are relevant to mechanisms of T-cell activation that require clustering or other reorganization of cell surface MHC class I molecules.

MATERIALS AND METHODS

Cells and antibodies

HeLa cells were cultured and maintained in Dulbecco's modified Eagle's medium (DME) (Gibco, Paisley) supplemented with fetal calf serum (FCS) (10% v/v), glutamine (2 mM), and streptomycin/ampicillin at 37°C in a humidified atmosphere of 7% CO_2. Trypsinized cells were seeded into eight-well LabTek chambers (Gibco) (5×10^3 cells/well) and cultured for 72 h before imaging. HOM-2, a B-lymphoblastoid cell line, was obtained from the Department of Immunology, The Royal London Hospital. The cells were maintained in Roswell Park Memorial Institute 1640 medium (Gibco, Paisley), supplemented with FCS (10% v/v), glutamine (2 mM), and streptomycin/ampicillin, at 37°C in a humidified atmosphere of 7% CO_2. IgG was prepared from ascites fluid (2 ml) (obtained from the London Hospital Medical College) containing W6/32, a panreactive class I monoclonal antibody, using a Protein G HiTrap column, and Fab fragments were prepared by papain digestion as described previously (Smith et al., 1998).

Preparation and high-performance liquid chromatography purification of an R-phycoerythrin-Fab conjugate

Fab fragments were purified by size-exclusion high-performance liquid chromatography (HPLC) and conjugated with the pyridyl disulfide derivative of PhyE (Molecular Probes, Eugene, OR) as described previously (Smith et al., 1998). Briefly, Fab fragments were dialyzed against sodium phosphate buffer (20 mM, pH 7.0) containing NaCl (0.1 M) and concentrated to 5 mg ml^{-1} with a centristart 1 device (10 kDa molecular mass exclusion limit) (Sartorius). Ten molar equivalents of a stock solution of succinimidyl *trans*-4-(*N*-maleimidyl-methyl)cyclohexane-1-carboxylate (5 mM) in dimethyl sulfoxide was added to the Fab (208 μg) and incubated for 2 h at room temperature. Excess succinimidyl *trans*-4-(*N*-maleimidyl-methyl)cyclohexane-1-carboxylate was removed by extensive dialysis against phosphate buffer. In parallel, the pyridyl disulfide derivative of PhyE (1 mg) (average 1.6 pyridyl disulphide derivatives per molecule) was incubated with solid dithiothreitol (DTT) (4 mg) for 15 min at room temperature, in the dark. Excess DTT was removed by extensive dialysis against phosphate buffer. The PhyE was then incubated with the Fab for 20 h at 4°C in the dark. Further reaction was stopped by the addition of a 20 molar excess of *N*-ethylmaleimide. PhyE and its conjugates were always handled in the dark.

The R-phycoerythrin-Fab conjugate (PhyE-Fab) was purified by size-exclusion chromatography on a BioRad 5000T HRLC controlled by a 486 PC. PhyE-Fab (300 μl) was loaded onto a Bio-Select SEC 250–5 column equilibrated with phosphate buffer (20 mM, pH 7.0) containing NaCl (0.1 M) at 0.1 ml min^{-1}. Fractions (100 μl) were collected and analyzed for activity by flow cytometry. Integration was performed using ValueChrom integration analysis software (BioRad).

Preparation of carboxylate-modified latex microspheres-Fab conjugates and a BSA conjugate

The microspheres were always handled in the dark. A stock solution of carboxylate-modified latex microspheres (CMLs), either 30 nm (8.49×10^{14} beads ml^{-1}) or 100 nm (4.5×10^{13} beads ml^{-1}) (Molecular Probes) in diameter, was sonicated for 5 min in a sonication bath and centrifuged to remove any agglomerates. An aliquot of the CMLs (0.5 ml, 10% solids) was added to 2-*N*-[morpholino]-ethanesulfonic acid (MES) buffer (9.5 ml, 50 mM, pH 6.0) in a glass test tube and sonicated for 5 min. A probe containing a 1:1 ratio of CML:Fab was required for the imaging experiment. The relative amounts of protein and microspheres required to produce a conjugate with this ratio was calculated by assuming that the proteins were spherical and packed on the bead surface in close hexagonal form. To prevent agglomeration of the CML and to prevent the unbound sites on the CMLs from sticking nonspecifically to cells or other proteins, BSA was conjugated to the CML together with the Fab. W6/32 Fab specific for class I MHC (39 μg for the 30-nm spheres, 2.06 μg for the 100-nm spheres) and BSA (6.42 mg for the 30-nm spheres, 1.86 mg for the 100-nm spheres) were added to the CMLs and incubated at room temperature for 15 min. 1-Ethyl-3-(3-dimethylaminopropyl)-carbodiimide) (10 mg) was added to the CMLs, and the pH adjusted to 6.5 $\pm$ 0.2 with dilute

NaOH. The CMLs were incubated with the Fab and BSA for 2 h at room temperature. Glycine (80 mg) was then added to the CML-Fab conjugates (CML30-Fab, CML100-Fab) and incubated for 30 min at room temperature. The CML-Fab conjugates were dialyzed against phosphate buffer (20 mM, pH 7.0) for 24 h at 4°C, with five changes of buffer, using cellulose ester dialysis tubing (500 kDa molecular mass exclusion limit) (Medicell International). The solution was centrifuged to remove any agglomerates. Sodium azide (0.05%) was added to the probe, which was stored in aliquots (1 ml) at 4°C in the dark. A 100-nm CML-BSA probe was similarly prepared that contained no Fab (CML100-BSA), for use as a control to monitor the nonspecific binding of BSA to a possible cell surface BSA receptor.

Flow cytometry

Analytical flow cytometry was employed to test whether the Fab retained specific binding activity after conjugation. HOM-2 cells were centrifuged at 300 × *g* for 5 min at room temperature and washed three times with PBS containing BSA (1%) and sodium azide (0.02%). PhyE-Fab and CML-Fab were incubated separately with the cells for 30 min at room temperature. The cells were then washed three times with PBS/BSA/NaN_3 and resuspended in PBS. The fluorescence was determined using an EPICS CS flow cytometer (Coulter Corporation), counting 10,000 cells per sample. The specific binding of the probes was examined by incubating the probes with the cells in the presence of a 10-fold excess of Fab.

Fluorescence digital imaging microscopy

Polylysine-coated slides

Glass microscope slides were incubated with alcoholic HCl (6% HCl (v/v), 70% ethanol (v/v)) in a glass slide holder for 1 h and then washed nine times with double-distilled H_2O (ddH_2O). The slides were then immersed in poly-L-lysine (0.01%) for 10 min at room temperature. After a brief rinse with ddH_2O, the slides were dried at 70°C for 25 min or overnight. Three dilutions of the fluorescent probe were prepared, and 15 μl was spread over the center of the microscope slide. The slides were left for 10 min at room temperature to allow the particles to settle and then gently washed twice with ddH_2O (30 μl); 15 μl ddH_2O was added to the slides, which were covered by a 0.17-mm-thick coverslip and sealed with silicone grease.

PhyE-Fab on cells

HeLa cells were seeded onto LabTek slides at a density of 5000 cells/well and cultured for 72 h before imaging. The cells were gently washed twice with PBS and then incubated with PhyE-Fab (10 μl) in PBS (90 μl) for 30 min at room temperature. The cells were gently washed three times with PBS, sealed with a coverslip, and transferred to a microscope stage maintained at 22°C. The absence of nonspecific binding was determined by incubating the cells with PhyE-Fab in the presence of a 10-fold excess of Fab.

CML-Fab on cells

The CML-Fab conjugates, both the stock solutions and any dilutions, were sonicated for 5 min and centrifuged at 5000 × *g* for 2 min before each experiment. The cells were gently washed twice with PBS at room temperature and incubated with the CML conjugate (100 μl, 1/500 dilution in PBS of stock conjugate) for 30 min at room temperature. The cells were washed three times gently with PBS, sealed with a coverslip, and transferred to a microscope stage maintained at 22°C. The absence of nonspecific binding was determined by incubating the cells with CML-Fab in the presence of a 10-fold excess of Fab.

Fluorescence microscopy

A Nikon Diaphot inverted fluorescence microscope was used for fluorescence digital imaging microscopy. The objective was either a 40× phase-contrast lens with numerical aperture 0.55 or a 60× oil immersion lens with a numerical aperture of 1.40. Illumination was provided by a 50-W mercury lamp, with a Vivid XF101 filter block (Omega Optical, Brattleboro, VT) with excitation and emission filters centered at 525 nm and 565 nm, respectively, and a dichroic mirror at 557 nm. A Peltier cooled charge-coupled device (CCD) camera (Wright Instruments, Enfield, England) was attached to the video port of the microscope, and the image was focused on an EEV CCD 02-06-1-206 back-illuminated detector (578 × 385 pixels; maximum quantum efficiency ~60%). Image acquisition, storage, and display were performed with Wright Instruments AT1 image control software.

The 40× phase-contrast lens was used to image the PhyE-Fab with exposure times of 2–5 s, at time intervals (Δt) of 20–60 s; exposure times of 300 ms at intervals down to $\Delta t = 4$ s were achieved with the 60× oil immersion objective. The 40× phase-contrast lens was used to image the CML-Fab conjugates and the CML-BSA conjugate. Typically, PhyE probes allowed 15 images to be obtained before photobleaching effects reduced the CCD signal-to-noise ratio to unacceptable levels. The latex beads were more photostable and could be tracked for more images; in practice, up to 30 images were usually recorded.

Data analysis

Tracking through fluorescent images

The methods used to quantify single particle imaging and tracking have been described in detail elsewhere (Anderson et al., 1992; Wilson et al., 1996). Briefly, diffraction-limited spots were fitted to a two-dimensional Gaussian peak, and the height above local background was the fluorescent intensity of that spot. Alternatively, the integrated signal (sum of all pixel counts under the peak) could be used to quantify the fluorescence. Single particle tracking was performed by matching the fitted central position coordinates of a Gaussian to one in the next image of a time lapse series by a "nearest spot with similar intensity" probability algorithm (Anderson et al., 1992). Tracks were then inspected manually, and any unreasonably wide spots (i.e., if the width of the fitted Gaussian differed from the diffraction-limited width by a significant amount, or if the spot width error was excessive) were excluded from the track; further analysis stages could then treat such events as a "missing image" for that track. Possible background motion of the slide with respect to the microscope was compensated for by subtracting the averaged apparent motion of a group of off-cell spots (if visible) or widely spaced on-cell spots.

Particle mobility analysis

Particle mobility was analyzed by constructing a histogram of the distance moved in a time interval $n\Delta t$ over all tracks on a cell, where n is the number of frames and Δt is the time interval between frames. The histograms were then fitted to the probability distribution for random diffusion:

$$P_n(r)\mathrm{d}r = N\frac{r}{2Dn\Delta t}\exp\left(\frac{-r^2}{4Dn\Delta t}\right)\mathrm{d}r \qquad (1)$$

Here D is the diffusion coefficient, r is the distance, and dr is the distance band over which the probability P_n is calculated; the fitting procedure treats D and the extensive parameter N (the number of jumps under the distribution) as variables. A set of such distance distributions with $n = 1, 2, \ldots$ may be fitted individually or globally as previously described (Wilson et al., 1996).

Individual tracks were analyzed by plotting the mean square displacement (MSD) against time interval (Anderson et al., 1992). MSD data were created by averaging all recorded jumps along the track for which the time interval was $n\Delta t$ ($n = 1, 2, \ldots$, up to half the total number of images).

Diffusion coefficients for individual tracks, designated D_{1-4}, were determined by fitting the first four points ($n = 1–4$) to the equation

$$\langle r^2 \rangle = 4D_{1-4}n\Delta t \quad (2)$$

Quantification of cellular ATP levels

To remove any contaminating phosphates, all glass and plasticware were incubated with 1 N HCl overnight, washed with ddH_2O, and oven dried. The experiments were performed in a sterile tissue culture environment with an ATP assay kit (Sigma Chemicals, Poole, England). HeLa cells were seeded onto four 24-well tissue culture plates (10,000 cells/well) and left to adhere for 48 h. The cells were washed twice with PBS (250 μl) and then incubated with a minimal volume of PBS (100 μl) or PBS containing sodium azide (10 mM), covered, and left at room temperature to mimic the conditions on the microscope stage during imaging. Each incubation was performed in triplicate. The contents of one vial of ATP assay mix (AM) was dissolved in ddH_20 (5 ml) by gentle swirling and left for 1 h on ice, in the dark, to dissolve completely. A 1:25 dilution of AM was prepared using assay mix dilution buffer dissolved in ddH_2O (50 ml) as the diluent. The ATP-releasing agent was diluted 1:10 with ddH_2O. AM (200 μl) was added to a scintillation tube, swirled around, and left to stand for 3 min. ATP-releasing agent (200 μl) and ddH_2O (100 μl) were added to the cells in each of the wells in one plate. The cells were agitated vigorously with a pipette, 200 μl of this mixture was added to the AM in the scintillation tube, and the emitted light was measured immediately with a scintillation counter. The assay was repeated on the remaining 24-well plates at 30-min intervals for 2 h.

Photostability assay

Photobleaching of the probes was assessed from the fluorescence intensities of eight tracked spots. Along each track j, the mean intensity above local background $\langle Z \rangle_j$ was calculated. At each time point t, the normalized intensity $Z(t)_j/\langle Z \rangle_j$ was averaged for the eight spots, giving mean normalized fluorescence as a function of time, $\langle Z(t) \rangle$. These values were then fitted to a single exponential decay to obtain the photobleaching time constant τ.

RESULTS

PhyE-Fab, CML100-Fab, and CML30-Fab probes

Probes for investigating the mobility of MHC class I receptors on the surface of HeLa cells were prepared by isolating Fab fragments of the anti-MHC class I monoclonal antibody W6/32 and conjugating them in a 1:1 molar ratio with either PhyE or fluorescent latex microspheres. The univalent PhyE-Fab probe was separated from free Fab, free PhyE, and higher valency PhyE-Fab conjugates by size exclusion HPLC, as previously described (Smith et al., 1998; Cherry et al., 1998). The CML-Fab probes were separated from free Fab by dialysis, but it was not possible to separate them from the free microspheres or any higher valency conjugates. The Fab and microspheres were mixed in a 1:1 molar ratio in an attempt to ensure that the major species present contained a 1:1 ratio of Fab to microspheres.

The specificity of the PhyE-Fab, CML100-Fab, and CML30-Fab probes for MHC class I receptors was tested by flow cytometry, using a B-lymphoblastoid cell line, HOM-2. Flow cytometric analysis of the PhyE-Fab probe showed a high fluorescence intensity (Fig. 1 *Aii*), which was greatly reduced upon the addition of a 10-fold excess of free Fab (Fig. 1 *Aiii*). Flow cytometric analysis of the CML100-Fab and CML30-Fab probes also showed a high fluorescence intensity (Fig. 1, *Bii* and *Cii*, respectively). However, incubation with a 10-fold excess of free Fab did not reduce the peak fluorescence of these probes (Fig. 1, *Biii* and *Ciii*), that is, the number of probe molecules bound per cell, but reduced the number of cells with that number of probe molecules bound. Similar observations were made during fluorescent digital imaging experiments where, in the presence of a 10-fold excess of Fab, most cells would exhibit no bound CML-Fab, but a small minority of cells would have very large quantities of CML-Fab bound. These cells could be damaged, although it is not clear why a similar phenomenon was not observed with R-PE.

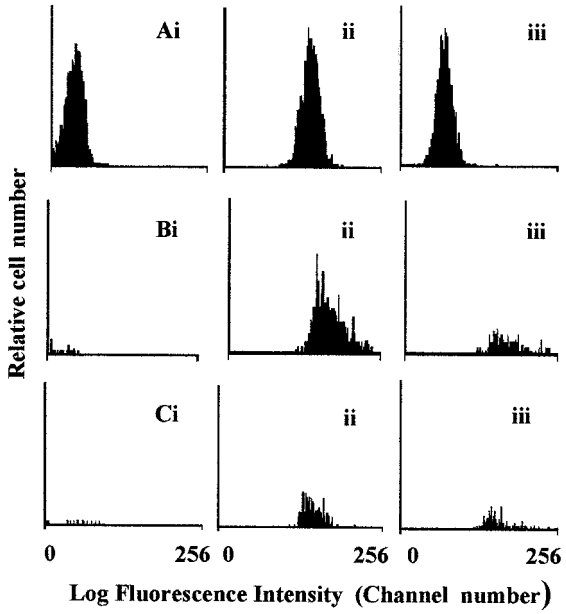

FIGURE 1 Flow cytometric analysis of the fluorescent probes PhyE-Fab (*A*), CML100-Fab (*B*), and CML30-Fab (*C*) binding to MHC class I molecules on HOM-2 cells. Cells were unlabeled (*i*), labeled with probe (*ii*), or labeled with probe in the presence of a 10-fold excess of free Fab (*iii*). Ten thousand cells were analyzed for fluorescence with an EPICS CS flow cytometer.

During the preparation of the CML30-Fab and CML100-Fab probes, excess BSA was used to bind the unoccupied sites on the microspheres. It is possible that BSA may cause the probes to bind nonspecifically to cells. To test this possibility, a CML100-BSA probe was prepared and incubated with HeLa cells. As shown in Fig. 2, the CML100-BSA probe did not bind to the cells, whereas the CML100-Fab probe did bind to the cells.

Cellular ATP analysis

The ATP levels of HeLa cells were measured in the presence and absence of sodium azide, under conditions similar to those experienced by cells during fluorescence digital imaging experiments, i.e., in the presence of a minimal volume of PBS, without the addition of CO_2 and at 22°C.

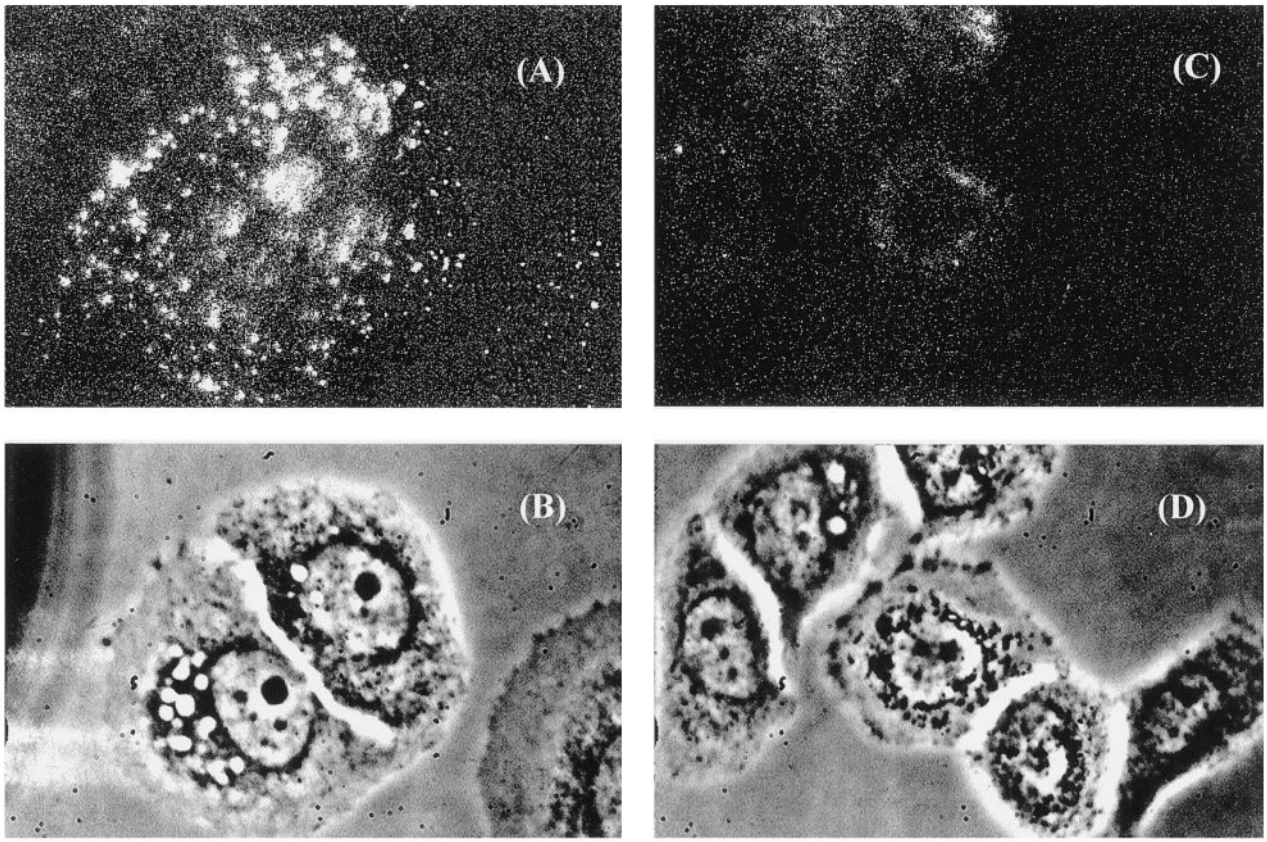

FIGURE 2 Digital fluorescence images of CML100-Fab (*A*) and CML100-BSA (*C*) bound to HeLa cells. The bright-field images of the same cells are shown in *B* and *D*, respectively.

As shown in Fig. 3, in the presence of sodium azide, over a period of 120 min, the cellular ATP levels fell by 90%. Over the same time period, the ATP levels were not significantly reduced under normal imaging conditions (i.e., in the absence of sodium azide).

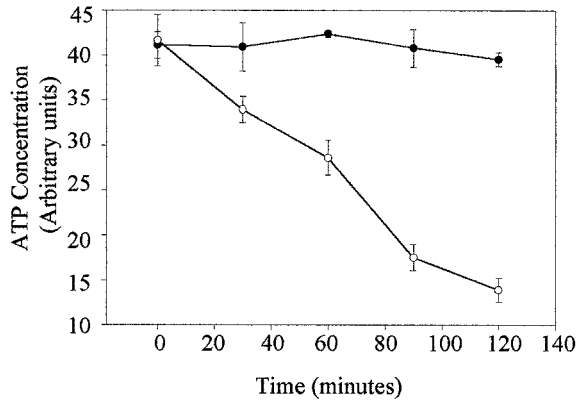

FIGURE 3 Analysis of the intracellular ATP concentration of HeLa cells incubated at 22°C for up to 2 h in PBS only (●) and in PBS with 10 mM sodium azide (○).

Mobility analysis of MHC class I molecules on HeLa cells

The PE-Fab, CML100-Fab, and CML30-Fab probes were used to study the mobility of MHC class I molecules on the surface of HeLa cells. Fig. 4 shows typical fluorescent images of these probes bound to HeLa cells at different exposure times.

In addition to individually dispersed particles, the majority of images contained bright patches of fluorescence that could not be resolved into single particles or small patches. Those fluorescent spots with widths close to the diffraction limit offered by the objective lens were analyzed as described earlier and tracked through time lapse images at intervals between 4 and 60 s, using exposure times between 300 ms and 5 s. Fig. 5 illustrates a representative sample of the tracks obtained with PhyE-Fab (Fig. 5 *A*) and CML100-Fab (Fig. 5 *B*) on cells and PhyE-Fab on poly-L-lysine-coated microscope slides (Fig. 5 *C*).

Plots of MSD against time for individual tracks were generally either linear or downward curving. The shapes of such plots may be indicative of different types of motion: downward curving plots occur for constrained diffusion and upward curving plots for directed motion (Anderson et al.,

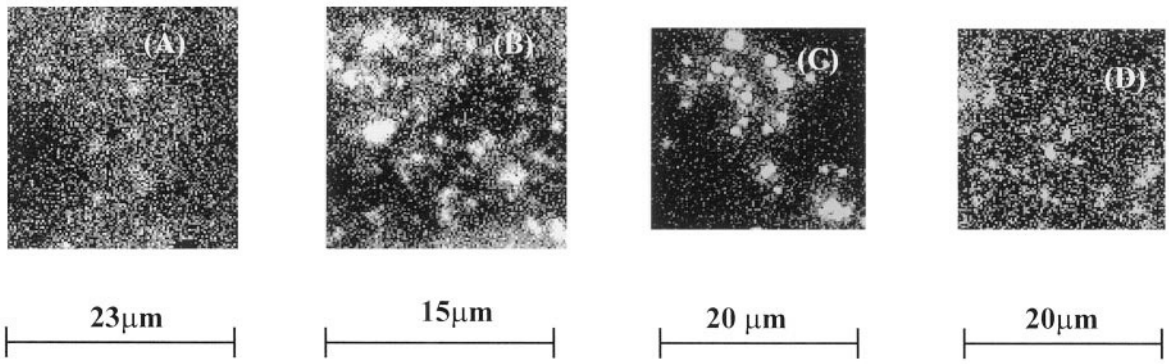

FIGURE 4 Digital fluorescent images of probes bound to MHC class I molecules on HeLa cells. (*A*) PhyE-Fab, 1-s exposure, 40× objective lens. (*B*) PhyE-Fab, 0.3-s exposure, 60× objective lens. (*C*) CML100-Fab, 5-s exposure, 40× objective lens. (*D*) CML100-Fab, 0.3-s exposure, 40× objective lens.

1992; Saxton and Jacobson, 1997). Whereas linear plots are predicted for random diffusion (Eq. 2), random movements can also produce significant numbers of upward or downward curving plots when there are limited numbers of time points (Saxton, 1993). Nevertheless, the lack of upward curving plots (<5%) indicates that there is little directed motion of MHC class I in the present experiments.

D_{1-4} values were determined for individual tracks and are plotted as histograms in Fig. 6. An upper limiting value for the diffusion coefficient of immobile spots was obtained from image sequences of PhyE-Fab adhering to polylysine-coated slides. These sequences were obtained under the same conditions as the on-cell data, and separate assessments were made for the different time intervals employed. Because of the improved photobleaching characteristics of the latex beads, the tracks could be followed for longer times, and hence the limit of mobility detection should be lower. However, the PhyE-Fab results were used to ensure that a pessimistic limit was chosen. Particles bound to polylysine-coated slides were tracked and the MSD values analyzed as described to obtain D_{1-4} parameters for each track. These showed a single-sided, approximately normal distribution, and a cutoff value was taken at the distribution peak value plus one standard deviation: 0.8×10^{-12} cm^2 s^{-1} for 4-s intervals and 0.33×10^{-12} cm^2 s^{-1} for 60-s intervals. When these cutoffs were applied to the cell data, none of the tracks for the PhyE-Fab probe were immobile, whereas 16% of CML100-Fab tracks were immobile at 4-s image intervals, and 35% were immobile at 60-s image intervals.

The decision to use this cutoff value could be justified by examining the results of an on-cell case in which two populations could be detected in the distance histograms (BLB170 in Table 1). Analysis of two distributions suggested that 37% of the jumps were of low mobility; in comparison, 40% of tracks were placed in the immobile category by applying the D_{1-4} cutoff value. If a higher cutoff was used (peak value plus two standard deviations), then 61% of the tracks were deemed immobile. The contrast between the immobile fractions for the two probes was still

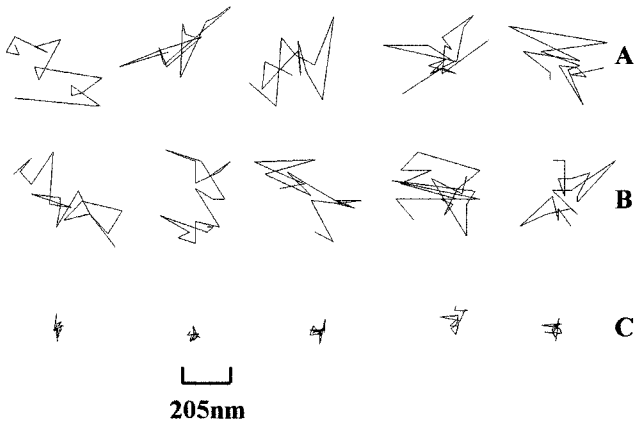

FIGURE 5 Examples of single particle tracks obtained with (*A*) PhyE-Fab bound to MHC class I molecules on HeLa cells. (*B*) CML100-Fab bound to MHC class I molecules on HeLa cells. (*C*) PhyE-Fab bound to a polylysine-coated microscope slide. Spots were linked through images obtained at ~4-s intervals.

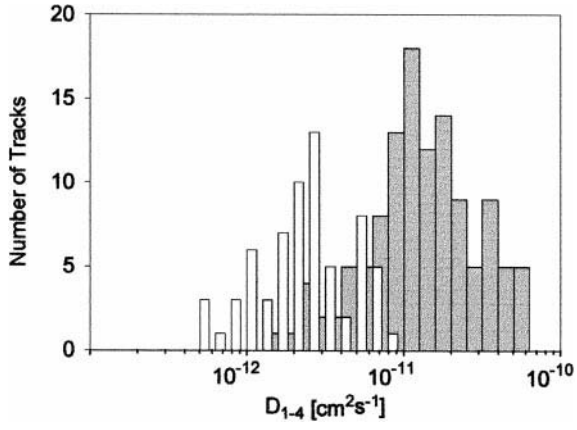

FIGURE 6 Histograms of D_{1-4} values for PhyE-Fab bound to MHC class I molecules on HeLa cells at 22°C. The gray bands represent data collected for three cells at intervals of 4.3 s between frames, using a 60× objective lens. The white bands (narrowed to show overlapping bands) contain data collected from three cells at 60-s intervals, using a 40× objective. Note the logarithmic axis and thus unequal bin widths.

TABLE 1 Analysis of SPT data for three fluorescent probes of MHC class I on HeLa cells

	Δt (s) and magnification	No. tracks analyzed	mean D_{1-4} (cm^2s^{-1}) $\times 10^{12}$	D_0 (cm^2s^{-1}) $\times 10^{12}$	Anomalous exponent α
CML30-Fab on CELL no.					
PS11A	60s 40×	40	1.6 ± 1.5	3.2 ± 1.0	0.73 ± 0.07
PS111	60s 40×	15	1.1 ± 1.1	2.2 ± 0.6	0.74 ± 0.07
PS40	30s 40×	106	0.2 ± 0.3	4.0 ± 2.1	0.08 ± 0.16
PS64	60s 40×	106	0.06 ± 0.3	2.2 ± 1.1	0.04 ± 0.13
			(Two mobility classes:	1.4 and 6.9	0.05 and 0.14)
PS85	60s 40×	165	0.4 ± 0.4	4.7 ± 3.1	0.54 ± 0.20
Mean value				3.3 ± 1.1	0.43 ± 0.34
CML100-Fab on CELL no.					
BLB07	11.4s 40×	33	2.5 ± 2.8	23.0 ± 10.0	0.10 ± 0.17
BLB34	4.7s 40×	23	16.0 ± 49.0	19.0 ± 12.0	0.39 ± 0.39
BLB58	4.8s 40×	42	5.0 ± 8.0	43.0 ± 9.0	0.05 ± 0.09
BLB81	4.6s 40×	16	8.0 ± 10.0	44.0 ± 23.0	0.23 ± 0.36
BLB126	60s 40×	33	0.50 ± 0.85	1.3 ± 0.5	0.30 ± 0.10
BLB149	60s 40×	23	2.3 ± 2.0	18.0 ± 5.0	0.46 ± 0.07
BLB170	60s 40×	67	0.9 ± 1.3	25.0 ± 25.0	−0.11 ± 0.87
			(Two mobility classes:	0.07 and 0.72	0.90 and 1.06)
BLB191	60s 40×	29	2.7 ± 2.1	9.3 ± 4.7	0.78 ± 0.15
Mean value				23. ± 15.0	0.28 ± 0.28
PhyE-Fab on CELL no.					
PE24	60s 40×	16	2.8 ± 1.9	40.0 ± 11.0	0.53 ± 0.07
PE46	60s 40×	21	3.0 ± 1.9	53.0 ± 27.0	0.46 ± 0.14
PE180	4.0s 40×	12	30.0 ± 18.0	40.0 ± 9.0	0.83 ± 0.11
PE192	4.0s 40×	11	35.0 ± 29.0	200.0 ± 70.0	0.19 ± 0.19
PE214	4.0s 40×	11	34.0 ± 20.0	91.0 ± 22.0	0.56 ± 0.12
PE225	5.0s 40×	19	16.0 ± 13.0	40.0 ± 12.0	0.43 ± 0.16
PE375	60s 40×	13	3.3 ± 2.2	42.0 ± 6.0	0.53 ± 0.03
PE461	4.3s 60×	37	13.0 ± 12.0	48.0 ± 16.0	0.40 ± 0.18
PE481	4.3s 60×	39	17.0 ± 10.0	44.0 ± 7.0	0.57 ± 0.07
PE502	4.3s 60×	41	18.0 ± 13.0	52.0 ± 15.0	0.64 ± 0.14
PE524	4.4s 60×	26	18.0 ± 13.0	66.0 ± 16.0	0.39 ± 0.12
PE545	4.3s 60×	38	21.0 ± 18.0	82.0 ± 26.0	0.31 ± 0.16
Mean value				67.0 ± 45.0	0.49 ± 0.16

Spots observed in time lapse image sequences were tracked, and plots of mean square displacement $\langle r^2 \rangle$ versus time increment $n\Delta t$ were created. The slope of the first four points gave the short-range diffusion coefficient D_{1-4} for each track. The table shows the mean value and standard deviation for each data set. Separately, all jumps in all tracks were collected into distance histograms across 1, 2, . . . , 5 image intervals, which were fitted by a theoretical diffusion distribution $P(r)dr$ to obtain a quasi-diffusion coefficient D for the corresponding time interval (see Fig. 7). Linear regression on log-log plots of these quasi-diffusion values against time provided the anomalous diffusion exponent α and its standard deviation, with the value of D at time 1 s, D_0 (see Fig. 8 and Eq. 3). In two cases the distance histogram obviously showed a two-component shape (see Fig. 10) and was additionally analyzed as such to give high- and low-mobility classes and their exponents.

evident for this higher cutoff: 1% for PhyE-Fab and 30% for CML100-Fab, using data obtained at 4-s intervals.

Typical distance histograms obtained with two different HeLa cells probed with PhyE-Fab are shown in Fig. 7 for three different values of $n\Delta t$ (Δt = 4.3 s for Fig. 7 *A–C* and 60 s for Fig. 7 *D–E*). Individual histograms are reasonably well fitted by Eq. 1. In particular, a second peak does not develop at longer times, as is the case when directed motion is present (Wilson et al., 1996). The absence of directed motion is consistent with the analysis of individual tracks. The values of D obtained by fitting the histograms with Eq. 1 decrease with increasing time increment. To further analyze the data, we assume a time-dependent diffusion coefficient (Feder et al., 1996):

$$D = D_0 t^{\alpha - 1} \tag{3}$$

or, by substitution into Eq. 2,

$$\langle r^2 \rangle = 4 D_0 t^{\alpha} \tag{4}$$

where t corresponds to $n\Delta t$ in Eq. 2, D_0 is a constant (the value of D at t = 1 s), and α is the anomalous diffusion exponent. Fig. 8 shows log-log plots of D against time interval, from which values of D_0 and α were obtained by

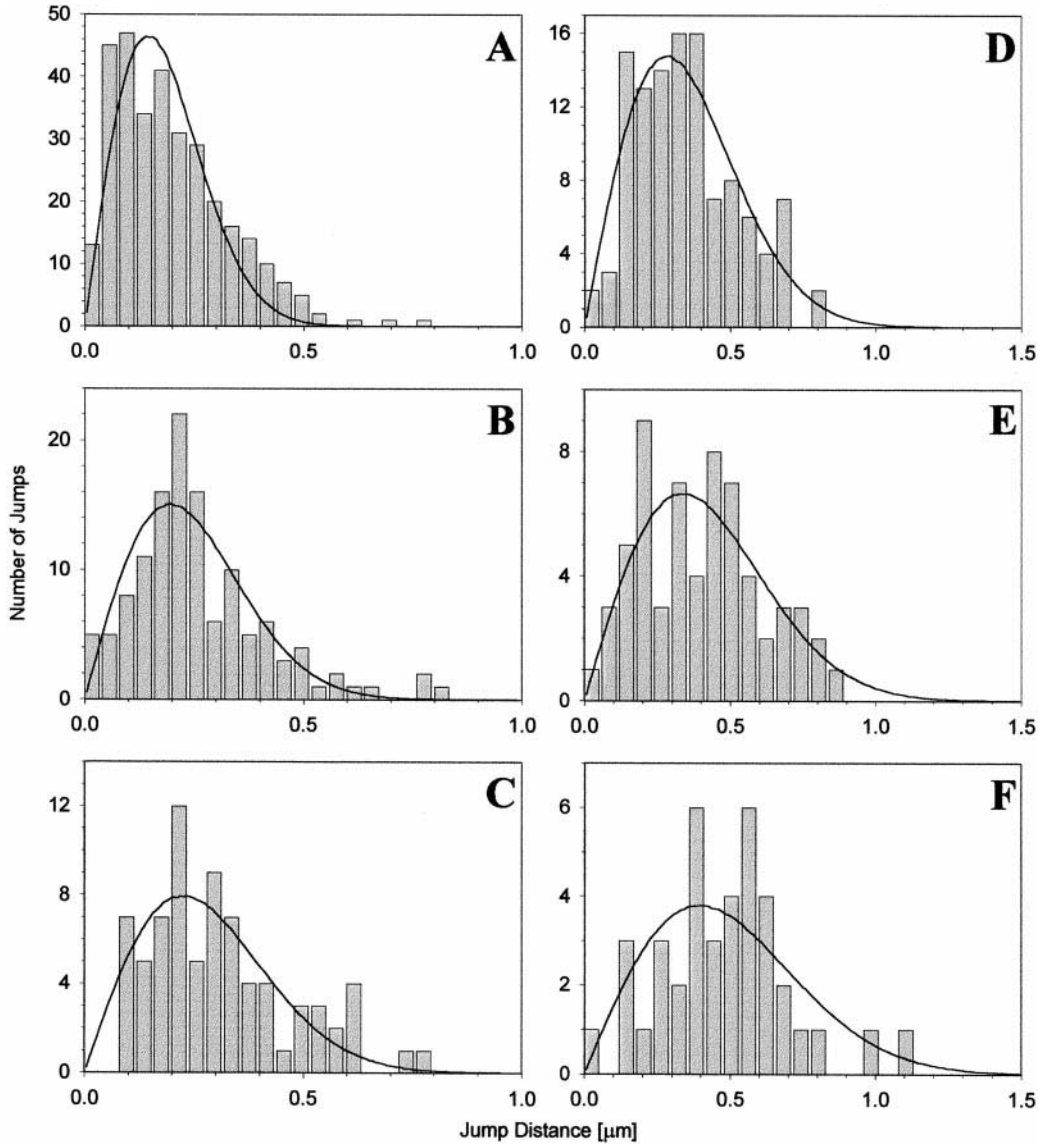

FIGURE 7 Distance histograms for the motion of PhyE-Fab bound to MHC class I molecules on HeLa cells at 22°C. (*A–C*) SPT was performed with a 60× objective lens, with an interval of 4.3 s between frames. Individual jumps across one (*A*), three (*B*), and five (*C*) time increments were combined, and the histograms were fitted by Eq. 1, giving, respectively, values of $D = (12.3 \pm 1.4)$, (6.5 ± 1.0), and $(4.1 \pm 0.7) \times 10^{-11}$ cm^2 s^{-1}. (*D–F*) SPT was performed with a 40× objective lens, with an interval of 60 s between frames. Individual jumps across one (*D*), three (*E*), and five (*F*) time increments were combined, and the histograms were fitted by Eq. 1, giving, respectively, values of $D = (6.7 \pm 0.5)$, (3.1 ± 0.4), and $(2.7 \pm 0.5) \times 10^{-12}$ cm^2 s^{-1}. Nonoverlapping jumps were used to construct the histograms; using overlapping jumps gave smoother histograms but essentially the same values of *D*.

linear regression. Plots for individual cells are shown to indicate cell-to-cell variability; the best fit parameters are given in Table 1. Averaging the values for individual cells gives $D_0 = (6.7 \pm 4.5) \times 10^{-11}$ cm^2 s^{-1} and $\alpha = 0.49 \pm 0.16$.

The tracking data for CML-labeled MHC class I were analyzed in a similar manner. Fig. 9 shows log-log plots of *D* against time interval for cells labeled with CML100-Fab. These results differ from those obtained with PhyE-Fab in a number of respects. The values of *D* are generally about two- to threefold smaller than the corresponding values for PhyE-Fab. There is also considerably greater cell-to-cell variation. Last, unlike measurements with PhyE-Fab, distance histograms for individual cells occasionally were poorly fitted by Eq. 1. An example is shown in Fig. 10, where the data can be fitted to two components, one essentially immobile and one exhibiting slow but apparently random diffusion.

Experiments performed with either CML30-Fab or CML-100 Fab gave similar results. The mean values of α were 0.28 ± 0.28 for CML-100 and 0.43 ± 0.34 for CML-30. The large uncertainties in these values reflects the large cell-to-cell variation observed with these probes.

Photobleaching of the probes

The photostability of the CML100-Fab and PhyE-Fab probes is compared in Fig. 11. Both probes photobleach

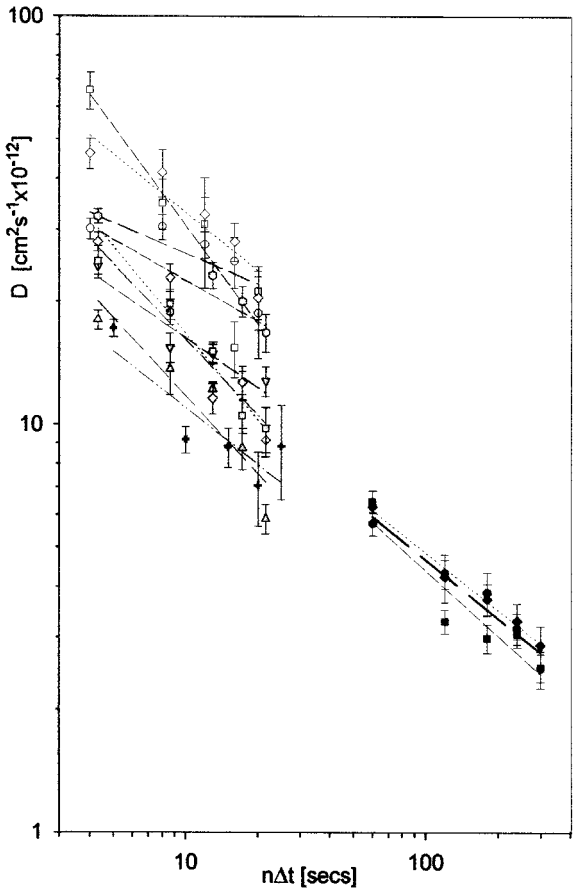

FIGURE 8 Plots of log D against log $n\Delta t$ for PhyE-Fab bound to MHC class I on HeLa cells at 22°C. D was determined for different time intervals, $n\Delta t$, as illustrated in Fig. 6. Each straight line corresponds to an individual cell with data points fitted by Eq. 3 to obtain D_0 and α. Values are given in Table 1.

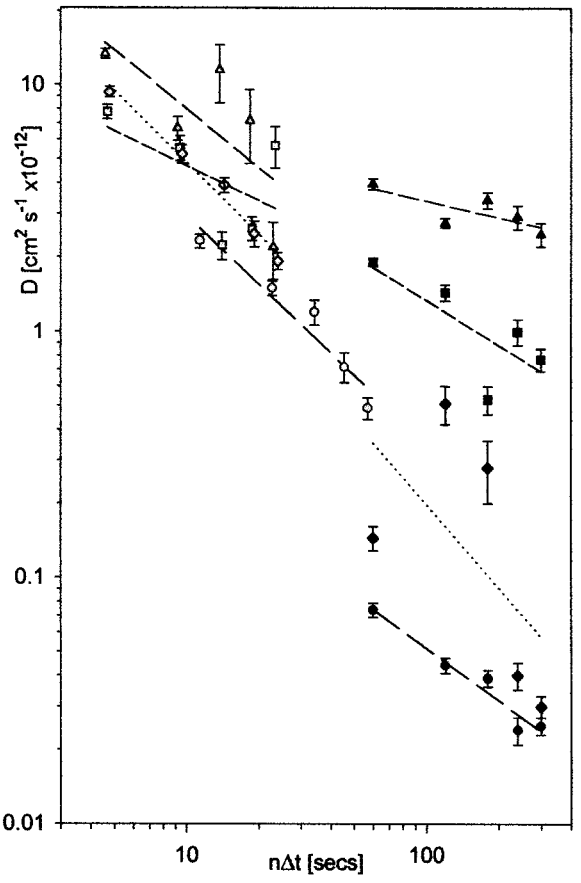

FIGURE 9 Plots of log D against log $n\Delta t$ for CML100-Fab bound to MHC class I on HeLa cells at 22°C. D was determined for different time intervals, $n\Delta t$, as illustrated in Fig. 6. Each straight line corresponds to an individual cell with data points fitted by Eq. 3 to obtain D_0 and α. Values are given in Table 1.

when subjected to a series of 300-ms exposures using the 60× oil-immersion objective lens. The fluorescent microspheres are more photostable; the intensity decays with $\tau =$ 8 s compared with 3.2 s for PhyE. These are worst-case data; with the 40× (air) objective lens, the microspheres did not bleach appreciably over a total exposure time of 100 s, whereas PhyE faded to half its initial intensity over ~50 s (data not shown).

DISCUSSION

Probes

In the present study, we have investigated two types of fluorescent particle for use in SPT experiments. Latex microspheres have the advantage of good photostability and are available in different sizes with a variety of fluorophores. Phycobiliproteins photobleach more readily but exhibit strong fluorescence relative to their small size. We find that the mobility of MHC class I on HeLa cells measured with CML-Fab probes is consistently lower than when measured with PhyE-Fab, and there are more immobile particles. This could be a size effect because PhyE is considerably smaller than the CMLs used for these experiments. Mobilities measured with CML30-Fab are, however, at least as low as those measured with CML100-Fab. Moreover, the 30-nm microspheres are comparable in size to the gold particles commonly employed for SPT, where higher mobilities have typically been observed, albeit with different receptors.

Another possible reason for the lower mobilities observed with CML-Fab is cross-linking of receptors. Although probes are designed to have an average stoichiometry of one Fab per bead, it is likely that there are significant numbers of beads with more than one Fab whose influence might be enhanced if they bind more strongly to the cell. In the case of PhyE-Fab, this problem is obviated because the relatively small size of PhyE makes it possible to separate a 1:1 mole fraction of PhyE:Fab by HPLC. Lee et al. (1991) have also raised concerns about the possible effects of probe multivalency in gold particle SPT.

In addition to Fab, the beads are coated with BSA, as is also the practice with gold particles. Although BSA can bind to cells, the binding sites are of relatively low affinity

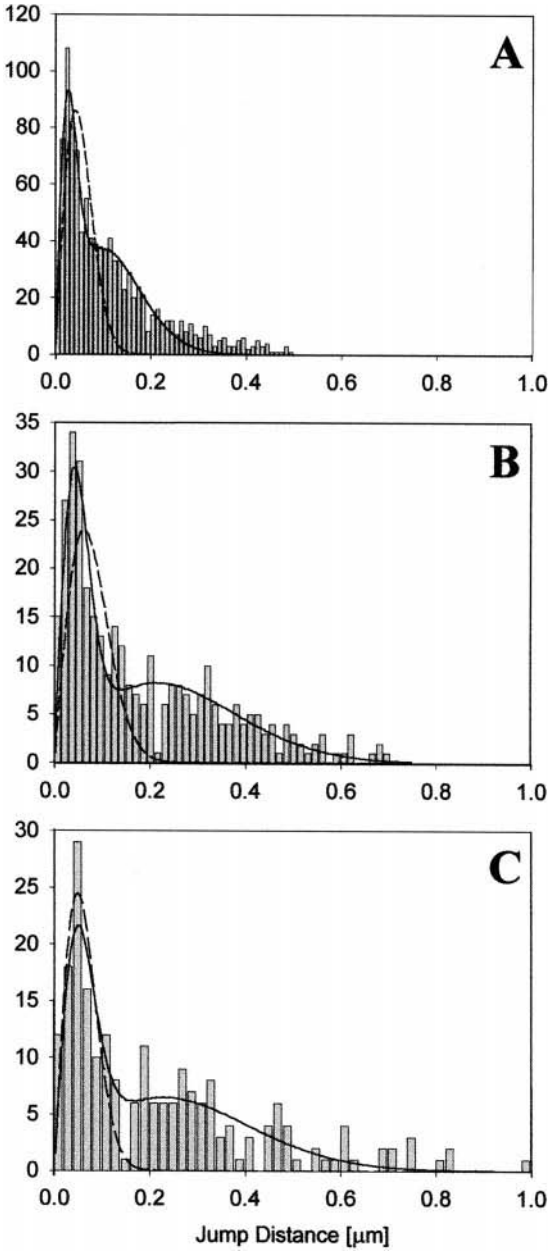

FIGURE 10 Distance histograms for the motion of CML100-Fab bound to MHC class I molecules on HeLa cells at 22°C, using a 40× objective lens, with an interval of 60 s between frames. Individual jumps across one (*A*), three (*B*), and five (*C*) time increments were combined, and the histograms were fitted by Eq. 1 for a single diffusion coefficient (– – –) or a modification of Eq. 1 to include two diffusion coefficients (——). Values of D for the two-component fit were (*A*) $(4.9 \pm 0.4) \times 10^{-14}$ cm^2 s^{-1} and $(8.8 \pm 0.7) \times 10^{-13}$ cm^2 s^{-1}; (*B*) $(4.8 \pm 0.4) \times 10^{-14}$ cm^2 s^{-1} and $(11.7 \pm 1.9) \times 10^{-13}$ cm^2 s^{-1}; and (*C*) $(3.2 \pm 0.4) \times 10^{-14}$ cm^2 s^{-1} and $(8.4 \pm 1.1) \times 10^{-13}$ cm^2 s^{-1}.

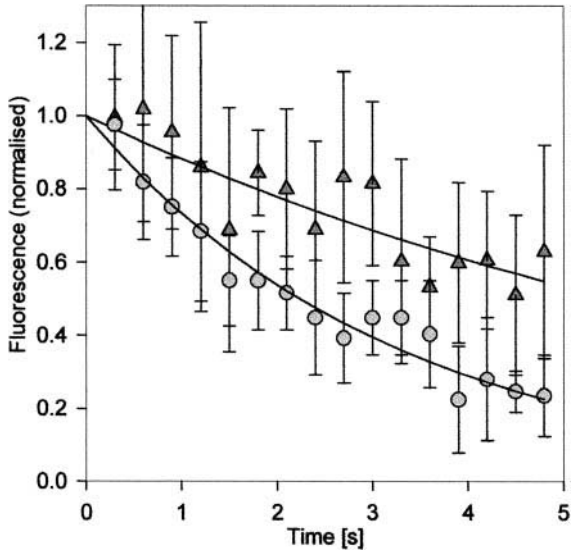

FIGURE 11 Photobleaching of PhyE-Fab (*circles*) and CML30-Fab (*triangles*) under the SPT experimental conditions, using a 60× oil-immersion objective lens, a 50-W mercury lamp, and a Vivid filter set. Data points and error bars are normalized mean and standard deviation for the intensities of eight fluorescent spots in time lapse images. The time axis is the sum of the exposure times without allowance for the shutter dead time before and after the camera exposure. Solid lines are best-fit exponential decays, $\tau = 8$ s (CML30) and 3.2 s (PE).

(Brunskill et al., 1997; Zucker et al., 1995). BSA-coated beads in the absence of Fab do not bind appreciably to cells under the conditions of the present experiments (Fig. 2). It is thus unlikely that additional binding by BSA is responsible for the low mobilities observed with CML-Fab.

Whatever the cause of the lower mobilities observed with fluorescent beads, R-phycoerythrin (or possibly other phycobiliproteins) is clearly the more appropriate particle for fluorescent SPT on cells. Its small size minimizes extracellular restrictions from steric effects; the ability to prepare a well-characterized univalent probe is a further advantage. Susceptibility to photobleaching limits the number of images that can be obtained in an SPT experiment, which in turn makes it more difficult to establish nonrandom movement for individual receptors. On the other hand, analysis of the movements of a population of receptors on a given cell, as discussed below, can give considerable insight into how receptors move on cell surfaces. For single molecule detection in model systems, a more photostable probe such as tetramethylrhodamine may be preferable (Schütz et al., 1997b).

Other experimental factors

SPT experiments previously reported by us for MHC class II on fibroblast cells were obtained with 5-s exposure times for individual images (Wilson et al., 1996). Conceivably, rapidly moving receptors could have remained undetected because of motional blurring of the particle images. A simulation of an SPT experiment reveals that a 1-s exposure time is sufficient to capture particles moving randomly with a diffusion coefficient of 10^{-9} cm^2 s^{-1} (Morrison, 1997). In the present study, we have employed exposure times down to 0.3 s and found no evidence for rapidly moving receptors that would not have been detected with the longer exposure times.

Thatte et al. (1996) have reported that ATP depletion can result in receptor immobilization. We have assayed ATP levels under the conditions of the SPT experiments and found that they are maintained for at least 120 min. It is thus unlikely that ATP depletion is a factor in the present study.

The photobleaching that occurs with PhyE could conceivably be accompanied by photooxidative cross-linking. This seems very unlikely, however, as the light intensities used in SPT are much less than in FRAP experiments, for which several studies have been performed to rule out this type of artefact (Peters and Scholz, 1991). Moreover, photooxidative effects would be expected to be more pronounced with PhyE than with CMLs, where photobleaching is much reduced, yet measured MHC class I mobilities are higher when the PhyE probe is used. Last, photooxidative cross-linking might be expected to have a progressive effect over the course of an SPT experiment. We have compared mobilities determined from images obtained during the first and second halves of an experiment and found no difference between the two halves.

Anomalous diffusion

Normal diffusion (Brownian motion) is characterized by an MSD that is proportional to time (Eq. 2). Studies of transport in disordered systems have revealed many instances of anomalous diffusion, where the MSD varies sublinearly with time as in Eq. 4 (Bouchaud and Georges, 1988). In this case, Eq. 1 is strictly no longer a valid description of the distance histograms. The form of $P(r, t)$ depends on the physical basis of anomalous diffusion (Bouchaud and Georges, 1990; Klafter et al., 1992). In addition to the analysis shown in Figs. 8 and 9, we have also analyzed the PhyE-Fab data by plotting log $(\langle r^2 \rangle / t)$ against log t, as recommended by Saxton (1994). These plots are very similar to Fig. 8 and yield a mean value of $\alpha = 0.49$. The mean value of $\langle r^2 \rangle$ at $t = 1$ s is 0.026 μm^2, which for normal diffusion would correspond to $D = 6.6 \times 10^{-11}$ cm^2 s^{-1}. Although the two methods give similar results, the advantage of using distance histograms is that they can reveal the presence of multiple components (Fig. 10 and Wilson et al., 1996) and provide a quasi-diffusion coefficient for a given time interval that can be compared with other measurement techniques. Plots of log $(\langle r^2 \rangle / t)$ against log t could give misleading results if there are subpopulations or outliers present with large values of r.

Experiments with both PhyE-Fab and CML-Fab probes indicate that anomalous diffusion of MHC class I on HeLa cells occurs over the time range 4–300 s. There are, however, quantitative differences in the results obtained with the two types of probe and in the reproducibility of data. For the reasons already discussed, we regard the PhyE-Fab data as the more reliable.

Webb and collaborators have previously interpreted SPT measurements with fluorescent LDL bound to LDL receptors or via Fab to IgE receptors by an anomalous diffusion model (Ghosh, 1991; Slattery, 1995; Feder et al., 1996). Data for LDL receptors from our laboratory are also consistent with anomalous diffusion (Anderson et al., 1992). A possible problem with LDL is that in our hands, it is difficult to eliminate nonspecific binding (see also Goldstein and Brown, 1977). This suggests that specifically bound LDL could bind weakly to other cellular components such as the extracellular matrix, which would complicate the interpretation of SPT data. PhyE, however, does not bind to cells in the absence of the attached Fab. This probe is also smaller (11 × 8 nm) than LDL (~22 nm diameter), thus reducing the possibility of steric hindrance. The present data thus provide stronger evidence for the existence of anomalous diffusion in cell membranes.

We observe essentially no immobile particles in the present PhyE-Fab tracking experiments with MHC class I. In contrast, FRAP experiments with cell surface receptors almost invariably indicate a significant immobile fraction. Edidin and Stroynowski (1991), for example, found immobile fractions between 0.47 and 0.68, depending on the size of the bleached spot, for MHC class I (H-2D) on mouse hepatoma cells. These experiments were interpreted by a domain model but could also be consistent with anomalous diffusion. Nagle (1992) proposed that anomalous diffusion might occur in cell membranes as a consequence of long-time tails in the jump rate of diffusing molecules. He analyzed the effect of long-tail kinetics on FRAP measurements and showed that the diffusion coefficient and immobile fraction determined by conventional means would depend on the length and time scale of the experiment. Subsequently, Feder et al. (1996) analyzed FRAP data for IgE receptors on rat basophilic leukemia cells both by the conventional model of random diffusion with an immobile fraction and by a model in which all receptors undergo anomalous diffusion. They found that the two models fitted the experimental data equally well. They also carried out simulations that suggest that FRAP experiments in general are unlikely to distinguish between normal and anomalous diffusion.

A distinguishing feature of the present studies is that anomalous diffusion is observed over a long time range. MHC class I molecules do not move far from their point of origin over times up to 20 min. Saxton (1994, 1995, 1996) employed Monte Carlo methods to investigate a variety of models of constrained diffusion. These models include diffusion within a domain, diffusion in the presence of random obstacles, and diffusion in the presence of binding sites with various properties. Binding models do not result in anomalous diffusion if the system is in thermal equilibrium, a condition that almost certainly applies to SPT experiments. A moderate concentration of immobile obstacles produces anomalous diffusion at short times with a cross-over to normal diffusion at long times (Saxton, 1994). The cross-over time increases with obstacle concentration up to the percolation threshold where diffusion becomes anomalous at all times. At the percolation threshold, the value of α is 0.7, higher than that measured for most of the cells investigated in the present experiments (Table 1). Above the percolation threshold, theoretical plots of log D (or log $(\langle r^2 \rangle / t)$) against log t are downward curving as α approaches zero at long times. Fitting such curves over a limited time range to a linear function could give values of α less than 0.7. Because of scatter of the experimental points and cell-

to-cell variability, however, it is difficult to establish whether downward curvature is in fact present in Figs. 8 and 9. Alternatively, low α values could arise from a dynamic arrangement of obstacles above the percolation threshold in which there is a wide range of escape times from local entrapment.

Evidence for the existence of obstacles to protein movement has been obtained for several cell types by laser tweezer experiments (Edidin et al., 1991, 1994; Sako and Kusumi, 1995; Sako et al., 1998; Kusumi et al., 1998). In these experiments, particles attached to receptors are dragged across the cell surface by the optical trap. Obstacles are detected when the particle falls off the tweezers. The histograms of distances dragged before encountering an obstacle are quite broad, suggesting an irregular arrangement of obstacles. It is proposed that the obstacles are cytoskeletal structures, because the average distance dragged is increased when the cytoplasmic domains of H-2L^d (Edidin et al., 1994) and E-cadherin (Sako et al., 1998) are shortened. Obstacles are also detected, however, although at somewhat larger separation, for H-2L^d with no cytoplasmic domain and for Qa2, a lipid-anchored MHC class I molecule. This suggests that clusters of immobile proteins or lipid domains could also cause intramembranous obstruction.

Different models of membrane protein mobility have been proposed on the basis of SPT experiments using gold particles. These studies are performed at video rates, thus permitting observation of particle movements in the subsecond time range. Sako and Kusumi (1994) propose a model in which receptors are confined to domains for short times but undergo long-range normal diffusion by domain hopping. They present strong evidence for such a mechanism for transferrin receptors on normal rat kidney fibroblastic cells, where they deduce domain diameters of a few hundred nanometers and average residence times of 30 s. Kusumi and Sako (1996) argue that domains are most probably formed by cytoskeletal structures. Simson et al. (1998) investigated the mobility of neural cell adhesion molecules on fibroblasts and muscle cells. They observed a subpopulation of particles that exhibited transient confinement in which normal diffusion was interspersed with short periods ($\sim$8 s) of confinement within regions of $\sim$300 nm diameter. Diffusion within the confinement zones was anomalous, as was the movement of a slowly diffusing subpopulation of particles. Sheets et al. (1997) propose that the confinement zones could be glycolipid-rich regions corresponding to detergent-insoluble membrane fractions observed in biochemical experiments (Simons and Ikonen, 1997). The evidence for lipid microdomains in cell membranes has recently been reviewed (Edidin, 1997).

It is, of course, likely that there are differences in mobility characteristics of different receptors in different cell types. Transformed cells in particular have a randomly interwoven meshwork of microfilaments rather than the microfilament bundles found in normal cells (Lin et al., 1984). This indicates a substantially altered cytoskeletal structure that could well influence constraints on receptor mobility. It is nevertheless of interest to consider the extent to which the present measurements and the gold particle SPT referred to above can be harmonized by taking into account the different time scales of the measurements. Kusumi and co-workers determined microscopic diffusion coefficients (D_{2-4}) from the MSDs at $2\Delta t$, $3\Delta\tau$ and $4\Delta t$, where Δt is the time interval between frames (Kusumi et al., 1993; Sako and Kusumi, 1994). For video rates, the time scale is thus $\sim$100 ms. Simson et al. (1998) determined short-range diffusion coefficients from the initial slope of MSD versus time plots. Values for microscopic diffusion coefficients from these various gold particle-SPT experiments are found in the range $(0.3–9) \times 10^{-10}$ cm^2 s^{-1}. In comparison, the anomalous diffusion parameters we obtain for MHC class I on HeLa cells with PhyE-Fab indicate that $D \approx 2 \times 10^{-10}$ cm^2 s^{-1} for a time interval of 100 ms, a value well within the range of the above measurements.

A modified domain-hopping model could account for the present results. We would not be able to detect rapid motion within a domain at the present time resolution, but long-time diffusion would be anomalous if there were a sufficiently broad distribution of escape times from individual domains. Simson et al. (1998) subdivided tracks of individual neural cell adhesion molecules, measured over 6.6 s, into mobile, slow, corralled, and immobile. They suggest that the results can be accounted for by a heterogeneous arrangement of obstacles in which obstacle-rich regions give rise to slow-diffusion or transient confinement while diffusion in other regions is unhindered. Only the mobile population exhibited normal diffusion; possibly all molecules would display anomalous diffusion over the longer times explored in the present study.

Functional implications

The present studies provide evidence for the existence of anomalous diffusion in cell membranes over long times. It will be important to extend SPT studies to more receptors and cell types to determine whether anomalous diffusion or other models are more appropriate for these time scales. Although various models can explain the immobile fraction seen in FRAP experiments, they differ markedly in their description of the movements of receptors over long times. Determining which model is applicable is thus critical for evaluating the kinetics of any functional process that requires lateral movements of receptors on the time scale of minutes or longer.

In the case of the MHC class I molecules studied here, there is considerable evidence from fluorescence resonance energy transfer experiments for clustering of these molecules on the cell surface (Chakrabarti et al., 1992; Catipovic et al., 1994; Matkó et al., 1994; Damjanovich et al., 1995; Vereb et al., 1995; Bacsó et al., 1996; Bodnár et al., 1996; Bene et al., 1997). It has been proposed that such clustering might enhance T-cell binding through multiple interactions involving CD8 (Bacsó et al., 1996). Anomalous diffusion could assist such a mechanism by maintaining a high local concentration of MHC class I over long times, particularly if class I molecules are preclustered when delivered to the plasma membrane.

A further interesting question is whether on antigen-presenting cells, MHC class I molecules bearing the appro-

priate peptide might be recruited to the vicinity of a bound T-cell to enhance the cell-cell interaction. Another possible role for diffusion in mediating the dimerization of T-cell receptor-MHC-peptide ternary complexes has been discussed by Weng and DeLisi (1998). Such mechanisms depend critically on the mean separation of receptors and precisely how they move in the plane of the membrane. An increase in surface density of MHC class I by up-regulation in infected cells could favor processes requiring dynamic molecular associations by reducing collision times. Weng and DeLisi (1998) additionally propose that infected cells could increase the diffusion coefficient of MHC molecules by modulating lipid fluidity. SPT experiments in general indicate, however, that lipid fluidity does not limit diffusion rates, except over very short distances (Kusumi and Sako, 1996; Saxton and Jacobson, 1997). A more likely mechanism, suggested by the present experiments, is that collision rates might be enhanced by increasing the value of α in infected cells. This could be achieved by structural changes involving, for example, the cytoskeleton. On the other hand, the cytoskeleton could play an active role by directing molecules into the appropriate region and thus enhancing rates of association. In view of these speculations, it would be of considerable interest to compare mobility and clustering of MHC class I molecules in healthy and infected cells.

This work was funded by the Biotechnology and Biological Sciences Research Council.

REFERENCES

Anderson, C. M., G. N. Georgiou, I. E. G. Morrison, G. V. W. Stevenson, and R. J. Cherry. 1992. Tracking of cell surface receptors by fluorescence digital imaging microscopy using a charge-coupled device camera: low-density lipoprotein and influenza virus receptor mobility at 4°C. *J. Cell Sci.* 101:415–425.

Bacsó, Z., L. Bene, A. Bodnár, J. Matkó, and S. Damjanovich. 1996. A photobleaching energy transfer analysis of CD8/MHC-I and LFA-1/CAM-1 interaction in CTL-target cell conjugates. *Immunol. Lett.* 54: 151–156.

Bene, L., J. Szöllösi, M. Balázs, L. Mátyus, R. Gáspár, M. Ameloot, R. E. Dale, and S. Damjanovich. 1997. Major histocompatibility complex class I protein conformation altered by transmembrane potential changes. *Cytometry.* 27:353–357.

Bjorkman, P. J., M. A. Saper, B. Samraoui, W. S. Bennett, J. L. Strominger, and D. C. Wiley. 1987. Structure of human class I histocompatibility antigen, HLA-A2. *Nature.* 329:506–512.

Bodnár, A., A. Jenei, L. Bene, S. Damjanovich, and J. Matkó. 1996. Modification of membrane cholesterol level affects expression and clustering of class I HLA molecules at the surface of JY lymphoblasts. *Immunol. Lett.* 54:221–226.

Bormann, B. J., and D. M. Engelman. 1992. Intramembrane helix-helix association in oligomerisation and transmembrane signaling. *Annu. Rev. Biophys. Biomol. Struct.* 21:223–242.

Bouchaud, J.-P. A., and A. Georges. 1988. The physical mechanisms of anomalous diffusion. *In* Disorder and Mixing. E. Guyon, J.-P. Nadal, and Y. Pomeau, editors. Kluwer Academic Publishers, Dordrecht, the Netherlands. 19–29.

Bouchaud, J.-P., and A. Georges. 1990. Anomalous diffusion in disordered media: statistical mechanisms, models, and physical applications. *Phys. Rep.* 195:127–193.

Brunskill, N. J., S. Nahorski, and J. Walls. 1997. Characteristics of albumin binding to opossum kidney cells and identification of potential receptors. *Pflugers Arch. Eur. J. Physiol.* 433:497–504.

Capps, G. G., B. E. Robinson, R. D. Lewis, and M. C. Zúñiga. 1993. In vivo dimeric association of class I MHC heavy chains. *J. Immunol.* 151:159–169.

Catipovic, B., G. Talluri, J. Oh, T. Y. Wei, X. M. Su, T. E. Johansen, M. Edidin, and J. P. Schneck. 1994. Analysis of the structure of empty and peptide-loaded major histocompatibility molecules at the cell surface. *J. Exp. Med.* 180:1753–1761.

Chakrabarti, A., J. Matkó, N. A. Rahman, B. G. Barisas, and M. Edidin. 1992. Self-association of class I major histocompatibility complex molecules in liposomes and cell-surface membranes. *Biochemistry.* 31: 7182–7189.

Cherry, R. J. 1992. Keeping track of cell surface receptors. *Trends Cell Biol.* 2:242–244.

Cherry, R. J., P. R. Smith, I. E. G. Morrison, M. Koukidou, K. M. Wilson, and N. Fernández. 1997. Mobility of cell surface MHC molecules investigated by single-particle fluorescent imaging. *Biochem. Soc. Trans.* 25:1097–1102.

Cherry, R. J., K. M. Wilson, K. Triantafilou, P. O'Toole, I. E. G. Morrison, P. R. Smith, and N. Fernández. 1998. Detection of dimers of dimers of HLA-DR on the surface of living cells by single particle fluorescence imaging. *J. Cell Biol.* 140:71–79.

Damjanovich, S., L. Trón, J. Szöllösi, R. Zidovetzki, W. C. Vaz, F. Regateiro, D. J. Arndt-Jovin, and T. M. Jovin. 1983. Distribution and mobility of murine histocompatibility H-2K^k antigen in the cytoplasmic membrane. *Proc. Natl. Acad. Sci. USA.* 80:5985–5989.

Damjanovich, S., G. Vereb, A. Schaper, A. Jenei, J. Matkó, J. P. P. Starink, G. Q. Fox, D. J. Arndt-Jovin, and T. M. Jovin. 1995. Structural hierarchy in the clustering of HLA class I molecules in the plasma membrane of human lymphoblastoid cells. *Proc. Natl. Acad. Sci. USA.* 92:1122–1126.

de Brabander, M., R. Nuydens, A. Ishihara, B. Holifield, K. Jacobson, and H. Geerts. 1991. Lateral diffusion and retrograde movements of individual cell surface components on single motile cells observed with Nanovid microscopy. *J. Cell Biol.* 112:1143–1150.

Edidin, M. 1997. Lipid microdomains in cell surface membranes. *Curr. Opin. Struct. Biol.* 7:528–532.

Edidin, M., S. C. Kuo, and M. P. Sheetz. 1991. Lateral movements of membrane glycoproteins restricted by dynamic cyoplasmic barriers. *Science.* 254:1379–1382.

Edidin, M., and I. Stroynowski. 1991. Differences between the lateral organisation of conventional and inositol phospholipid-anchored membrane proteins. A further definition of micrometer scale membrane domains. *J. Cell Biol.* 112:1143–1150.

Edidin, M., M. C. Zúñiga, and M. P. Sheetz. 1994. Truncation mutants define and locate cytoplasmic barriers to lateral mobility of membrane glycoproteins. *Proc. Natl. Acad. Sci. USA.* 91:3378–3382.

Feder, T. J., I. Brustmascher, J. B. Slattery, B. Baird, and W. W. Webb. 1996. Constrained diffusion or immobile fraction on cell surfaces—a new interpretation. *Biophys. J.* 70:2767–2773.

Fernández, N., M. Kurpisz, M. Labeta, J. Sachs, and G. Pawelec. 1992. A ligand epitope in vitro analysis of major histocompatibility determinants expressed on B and T lymphocytes. *Immunology.* 77:116–122.

Ghosh, R. N. 1991. Mobility and clustering of individual low-density lipoprotein receptor molecules on the surface of human skin fibroblasts. Ph.D. thesis, Cornell University.

Ghosh, R. N., and W. W. Webb. 1990. Evidence for intramembrane constraints to cell surface LDL receptor motion. *Biophys. J.* 57:286a.

Ghosh, R. N., and W. W. Webb. 1994. Automated detection and tracking of individual and clustered cell surface low density lipoprotein receptor molecules. *Biophys. J.* 66:1301–131.

Goldstein, J. L., and M. S. Brown. 1977. The low-density lipoprotein pathway and its relation to atherosclerosis. *Annu. Rev. Biochem.* 46: 897–930.

Gross, D. J., and W. W. Webb. 1988. Cell surface clustering and mobility of the liganded LDL receptor measured by digital video fluorescence

microscopy. *In* Spectroscopic Membrane Probes, Vol. II, L. M. Loew, editor. CRC Press, Boca Raton, FL. 9–45.

Heldin, C. H. 1995. Dimerisation of cell-surface receptors in signal transduction. *Cell.* 80:213–223.

Hicks, B. W., and K. J. Angelides. 1995. Tracking movements of lipids and Thy-1 molecules in the plasmalemma of living fibroblasts by fluorescence video microscopy with nanometer scale precision. *J. Membr. Biol.* 144:231–244.

Jovin, T., and W. L. C. Vaz. 1989. Rotational and translational diffusion in membranes measured by fluorescence and phosphorescence methods. *Methods Enzymol.* 172:471–573.

Klafter, J., M. F. Shlesinger, G. Zumofen, and A. Blumen. 1992. Scale invariance in anomalous diffusion. *Philos. Mag. B.* 65:755–765.

Kusumi, A., and Y. Sako. 1996. Cell-surface organisation by the membrane skeleton. *Curr. Opin. Cell Biol.* 8:566–574.

Kusumi, A., Y. Sako, T. Fujiwara, and M. Tomishige. 1998. Applications of laser tweezers to studies of fences and tethers of the membrane skeleton that regulate the movements of plasma membrane proteins. *Methods Cell Biol.* 55:173–194.

Kusumi, A., Y. Sako, and M. Yamamoto. 1993. Confined lateral diffusion of membrane receptors as studied by single particle tracking (Nanovid microscopy). Effects of calcium induced differentiation in cultured epithelial cells. *Biophys. J.* 65:2021–2040.

Lee, G. M., A. Ishihara, and K. A. Jacobson. 1991. Direct observation of Brownian motion of lipids in membranes. *Proc. Natl. Acad. Sci. USA.* 88:6274–7278.

Lin, J. J.-C., S. Yamashiro-Matsumura, and F. Matsumura. 1984. Microfilamemts in normal and transformed cells: changes in the multiple forms of tropomysin. *In* The Transformed Phenotype. A. J. Levine, G. F. V. Woude, W. C. Topp, and J. D. Watson, editors. Cold Spring Harbor Laboratory, Cold Spring Harbor, New York. 57–65.

Matkó, J., Y. Bushkin, T. Wei, and M. Edidin. 1994. Clustering of class I HLA molecules on the surfaces of activated and transformed human cells. *J. Immunol.* 152:3353–3360.

Metzger, H. 1992. Transmembrane signaling—the joy of aggregation. *J. Immunol.* 149:1477–1487.

Morrison, I. E. G. 1997. Diffusion in cell membranes: single-particle tracking by fluorescence microscopy and its application to the low density lipoprotein receptor. Ph.D. Thesis, University of Essex, Essex, England.

Nagle, J. F. 1992. Long-tail kinetics in biophysics? *Biophys. J.* 63:366–370.

Peters, R., and M. Scholz. 1991. Fluorescence photobleaching techniques. *In* New Techniques of Optical Microscopy and Microspectroscopy. R. J. Cherry, editor. Macmillan, New York. 199–228.

Qiu, Y., W. F. Wade, D. A. Roess, and B. G. Barisas. 1996. Lateral dynamics of major histocompatibility complex class II molecules bound with agonist peptide or altered peptide ligands. *Immunol. Lett.* 53:19–23.

Sako, Y., and A. Kusumi. 1994. Compartmentalised structure of the plasma membrane for receptor movements as revealed by a nanometer-level motion analysis. *J. Cell Biol.* 125:1251–1264.

Sako, Y., and A. Kusumi. 1995. Barriers for lateral diffusion of transferrin receptor in the plasma membrane as characterised by receptor dragging by laser tweezers: fence versus tether. *J. Cell Biol.* 129:1559–1574.

Sako, Y., A. Nagafuchi, S. Tsukita, M. Takeichi, and A. Kusumi. 1998. Cytoplasmic regulation of the movement of E-cadherin on the free cell surface as studied by optical tweezers and single particle tracking: corraling and tethering by the membrane skeleton. *J. Cell Biol.* 140: 1227–1240.

Saxton, M. J. 1993. Lateral diffusion in an archipelago: single particle diffusion. *Biophys. J.* 64:1766–1780.

Saxton, M. 1994. Anomalous diffusion due to obstacles: a Monte Carlo study. *Biophys. J.* 66:394–401.

Saxton, M. 1995. Single particle tracking—effects of corrals. *Biophys. J.* 69:389–398.

Saxton, M. 1996. Anomalous diffusion due to binding—a Monte Carlo study. *Biophys. J.* 70:1250–1262.

Saxton, M. J., and K. Jacobson. 1997. Single-particle tracking: applications to membrane dynamics. *Annu. Rev. Biophys. Biomol. Struct.* 26:373–399.

Schmidt, T., G. J. Schütz, W. Baumgartner, H. J. Gruber, and H. Schindler. 1996. Imaging of single molecule diffusion. *Proc. Natl. Acad. Sci. USA.* 93:2926–2929.

Schram, V., J.-F. Tocanne, and A. Lopez. 1994. Influence of obstacles on lipid lateral diffusion: computer simulation of FRAP experiments and application to proteoliposomes and biomembranes. *Eur. Biophys. J.* 23:337–348.

Schütz, G. J., H. J. Gruber, H. Schindler, and T. Schmidt. 1997b. Fluorophores for single molecule spectroscopy. *J. Luminescence.* 72:18–21.

Schütz, G. J., H. Schindler, and T. Schmidt. 1997a. Single-molecule microscopy on model membranes reveals anomalous diffusion. *Biophys. J.* 73:1073–1080.

Sheets, E. D., G. M. Lee, R. Simson, and K. Jacobson. 1997. Transient confinement of a glycosylphosphatidylinositol-anchored protein in the plasma membrane. *Biochemistry.* 36:12449–12458.

Sheets, E. D., R. Simson, and K. Jacobson. 1995. New insights into membrane dynamics from the analysis of cell surface interactions by physical methods. *Curr. Opin. Cell Biol.* 7:707–714.

Sheetz, M. P., S. Turney, H. Qian, and E. L. Elson. 1989. Nanometer-level analysis demonstrates that lipid flow does not drive membrane glycoprotein movement. *Nature.* 340:284–288.

Slattery, J. P. 1995. Lateral mobility of FceRI on rat basophilic leukaemia cells as measured by single particle tracking using a novel bright fluorescent probe. Ph.D thesis. Cornell University.

Simons, K., and E. Ikonen. 1997. Functional rafts in cell membranes. *Nature.* 387:569–572.

Simson, R., E. D. Sheets, and K. Jacobson. 1995. Detection of temporary lateral confinement of membrane proteins using single-particle tracking analysis. *Biophys. J.* 69:989–993.

Simson, R., B. Yang, S. E. Moore, P. Doherty, F. S. Walsh, and K. A. Jacobson. 1998. Structural mosaicism on the submicron scale in the plasma membrane. *Biophys. J.* 74:297–308.

Smith, P. R., K. M. Wilson, I. E. G. Morrison, R. J. Cherry, and N. Fernández. 1998. Imaging of individual cell surface MHC antigens using fluorescent particles. *In* MHC: Biochemistry and Genetics. N. Fernández and G. Butcher, editors. Practical Approach Series, Oxford University Press, London. 131–151.

Thatte, S. T., K. R. Bridges, and D. E. Golan. 1996. ATP depletion causes translational immobilization of cell surface transferrin receptors in K562 cells. *J Cell. Physiol.* 166:446–452.

Vereb, G., L. Mátyus, L. Bene, G. Panyi, Z. Bacsó, M. Balázs, J. Matkó, J Szöllösi, R. Gáspár, S. Damjanovich, R. E. Dale, C. Pieri, and M. Ameloot, M. 1995. Plasma-membrane-bound macromolecules are dynamically aggregated to form nonrandom codistribution patterns of selected functional elements—do pattern-recognition processes govern antigen presentation and intercellular interactions? *J. Mol. Recognit.* 8:237–246.

Wade, W. F., J. H. Freed, and M. Edidin. 1989. Translational diffusion of class II major histocompatibility complex molecules is constrained by their cytoplasmic domains. *J. Cell Biol.* 109:3325–3331.

Wang, Y., J. D. Silverman, and L. Cao. 1994. Single particle tracking of surface receptor movement during cell division. *J. Cell Biol.* 127:963–971.

Weiss, A., and D. R. Littman. 1994. Signal transduction by lymphocyte antigen receptors. *Cell.* 76:263–274.

Weng, Z., and C. DeLisi. 1998. Toward a predictive understanding of molecular recognition. *Immunol. Rev.* 163:251–266.

Wilson, K. M., I. E. G. Morrison, P. R. Smith, N. Fernández, and R. J. Cherry. 1996. Single particle tracking of cell-surface HLA-DR molecules using R-phycoerythrin labelled monoclonal antibodies and fluorescence digital imaging. *J. Cell Sci.* 109:2101–2109.

Zhang, F., G. M. Lee, and K. Jacobson. 1993. Protein lateral mobility as a reflection of membrane microstructure. *Bioessays.* 15:579–588.

Zucker, S. D., W. Goessling, and J. L. Gollan. 1995. Kinetics of bilirubin transfer between serum albumin and membrane vesicles—insight into the mechanism of organic anion delivery to the hepatocyte plasma membrane. *J. Biol. Chem.* 270:1074–1081.